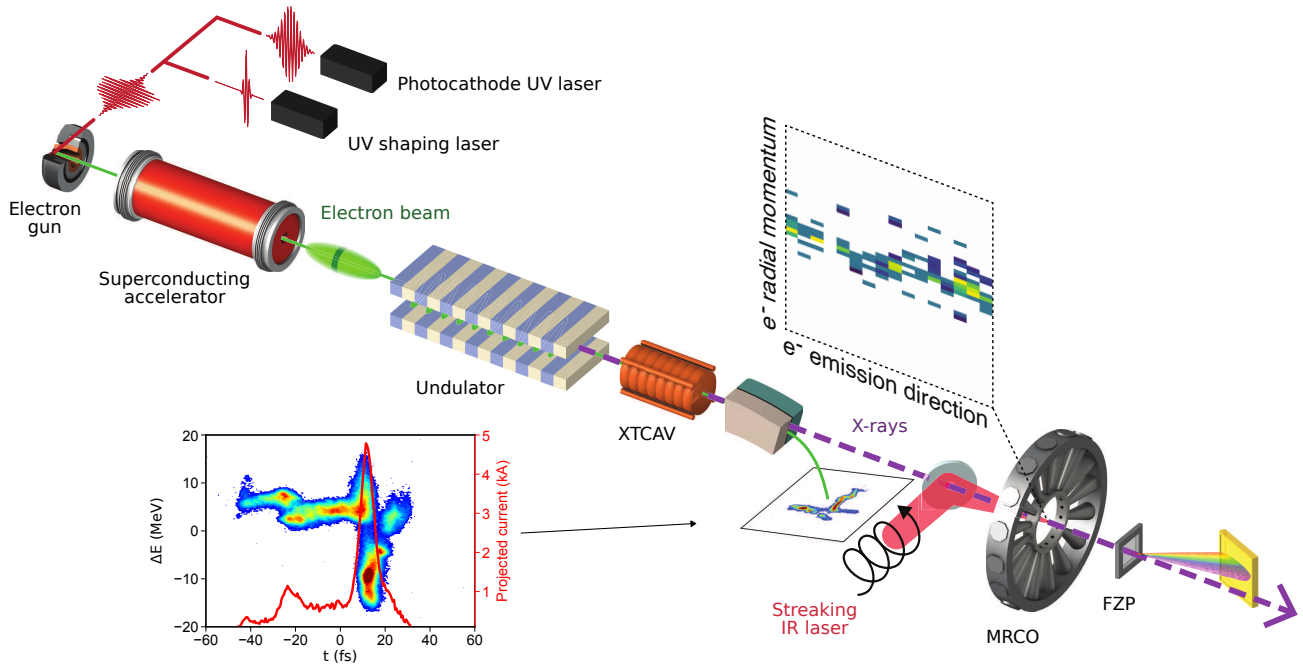

FIG. 1: **Schematic of experimental setup.** A short UV laser pulse is overlapped with the photocathode UV laser pulse, which then illuminates the photocathode at the electron gun and generates an electron beam with a slight density perturbation. The beam is then accelerated and compressed in the LCLS-II superconducting accelerator before entering the undulator section to generate attosecond X-ray pulses. After the undulator, the electron beam is deflected to an X-band transverse cavity (XTCAV) for longitudinal phase space measurement while the X-rays continue down the beamline. The X-rays photoionize a gas jet in the interaction region of a circular array of electron spectrometers (labeled MRCO) to generate photoelectrons, which are streaked with an overlapping circularly polarized infrared laser. After interaction, the X-ray pulses are diagnosed with a Fresnel zone-plate spectrometer (FZP).

with respect to the mirror surface. To ensure mirror reflectivity of hard x-ray photons, grazing incidence geometry is used. In the experiment, we fixed $\theta_1 = \theta_2 = 0.2°$, while M3 and M4, parallel and fixed with respect to each other, were rotated together over an angular range of $\theta_{34} = 0.15° - 0.25°$ for delay time adjustment. The measurements reported below were performed at a photon energy of 9.05 keV, with the system throughput measured above 80% across the full operating angles. The resulting time separation Δt between the delayed and fixed branches is therefore given by

$$\Delta t = \frac{d \sin \theta_{34}}{c \cos \theta_1} - \frac{d \tan \theta_1}{c}, \tag{1}$$

where c is the speed of light. The delay time coverage is plotted in Fig. 1 (b). The setup covers a delay range of 13.4 fs, with a 0.1 mdeg change in $\theta_{3,4}$ corresponding to a nominal delay adjustment of 13.4 as.

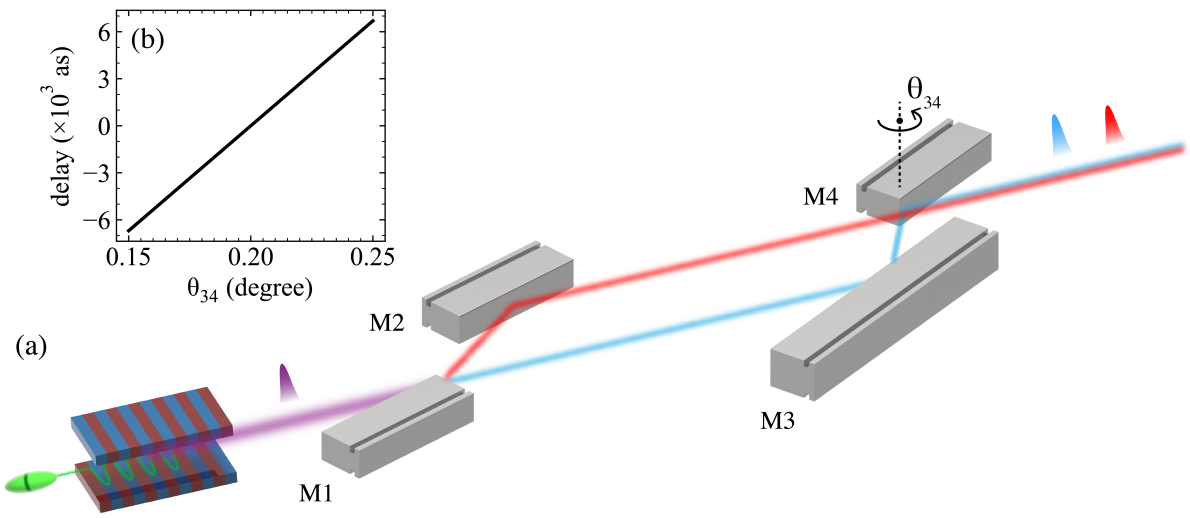

Figure 1: **Hard x-ray attosecond delay line.** (a) Schematic of the attosecond delay line consisting of four x-ray mirrors (M1 - M4). Delay is adjusted by rotating M3 and M4 together, with the rotation center located at the upstream edge of M4. The mirror operating angles are exaggerated for illustration. (b) Time separation, i.e., delay between the two output pulses as a function of the rotation angle θ_{34}.

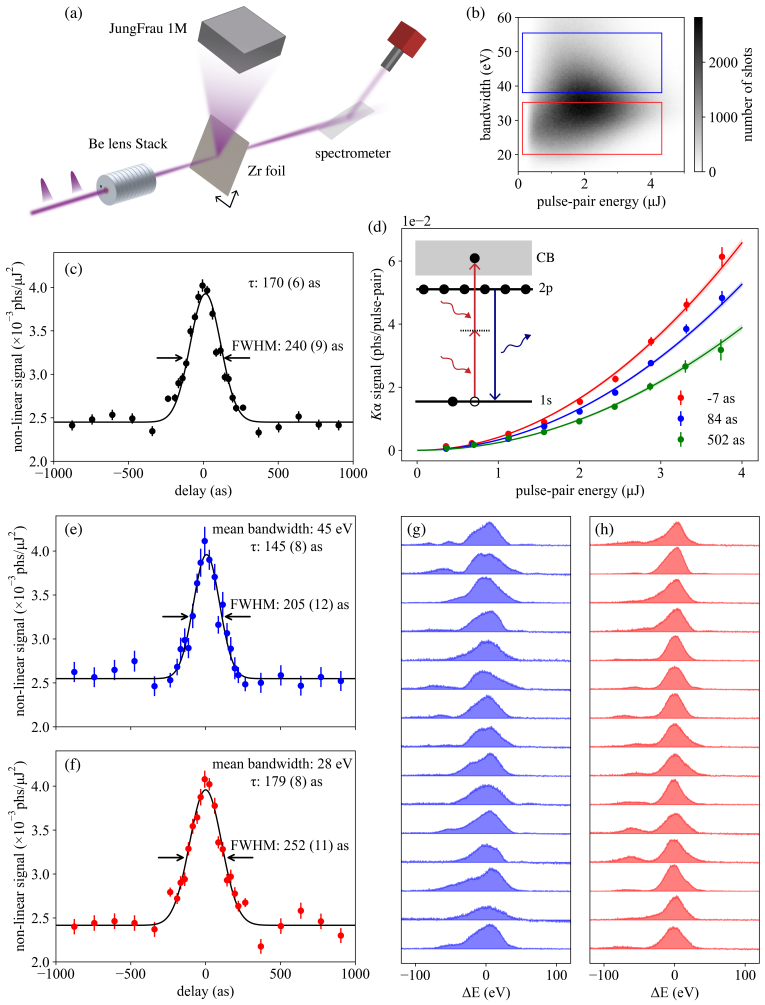

Figure 3: **Pulse duration measurement of attosecond hard x-ray pulses.** (a) Setup for the intensity autocorrelation-based pulse duration measurement. (b) Histograms of the pulse-pair energy at the sample plane and the bandwidth measured using the spectrometer shown in (a). (c) Intensity autocorrelation trace obtained using all the pulses displayed in (b). (d) Quadratic dependence of the Zr K_α fluorescence signal and the pulse pair energy at selected delays, corresponding to near time zero, half-maximum and long delays. The solid lines represent the nonlinear signal extracted and shown in (c). Inset: atomic transition diagram illustrating the non-sequential two-photon absorption of Zr. (e, f) Intensity autocorrelation time traces sorted by bandwidth, with average spectral widths of 45 eV and 28 eV, corresponding to the pulses highlighted by the blue and red boxes in (b), respectively. Representative spectra corresponding to these two bandwidths are shown in (g) and (h). For panels (c, e, f), the black solid lines indicate Gaussian fits to the time trace, and the fitted FWHM pulse duration values denoted by τ are displayed. The values in brackets give the standard error (1σ) of the fit.